

Appendix: Excess Temperature of the Yellowstone Plume

D.L. Schutt and K. Dueker

Section 1.0 Model Parameterization

To estimate the excess temperature of the Yellowstone plume, we construct a simple 1-D model of the crust and upper mantle along the hotspot track (Fig. 2). For a given plume excess temperature and grain size, melt porosity is estimated, and S-wave velocity with depth is predicted. S-wave velocity as a function of depth is then converted to phase velocity as a function of wave period (Saito, 1988), and these predicted phase velocities are compared with observations (Schutt et al., 2008).

For a range of excess temperatures and grain sizes, we test the null hypothesis that the predicted phase velocities are consistent with the observed phase velocities. The chi-squared values presented in Figs. 2, A1-3 represent the probability that the null hypothesis is violated: that is are the observed phase velocities consistent with the posited excess temperature and grain size.

The velocity model is constructed of four layers: 1) The crustal layer thickness and shear-wave velocity are constrained via inversion of the 15-40s wave period YHT phase velocity data and *P* to *S* conversion times from the crust-mantle boundary (Schutt et al., 2008; Yuan et al., in preparation) Although crustal thickness ranges from 38 to 53 km beneath the Yellowstone seismic array, the crustal thickness and mean crustal velocity are reasonably uniform (41–44 km) along the eastern Snake River Plain. 2) The mantle lithosphere layer is fixed at 8 km thickness and 4.2 km/s based on our velocity profiles (Fig. 2; also see Figure 15 in (Schutt et al., 2008)). This thin and low velocity mantle lid is consistent with the high surface heat flow (Blackwell et al., 1991) and the low lithospheric flexural rigidity (McQuarrie and Rodgers, 1998). Noteworthy is that a layer of Archean mantle lithosphere is required to explain the geochemical signatures of the late-stage basalt fields (Lum et al., 1989). 3) A layer of “plume” mantle is placed directly below the lithosphere. This represents material that has upwelled under Yellowstone Park and then has been sheared to the SW by North America Plate motion (i.e. the hot mantle under the eastern Snake River Plain). For most runs, the thickness of the plume layer is fixed at 60 km which is consistent with isostatic considerations (Schutt and Humphreys, 2004), P- and S-wave tomography (Schutt and Humphreys, 2004; Waite et al., 2006; Yuan and Dueker, 2005), the resolution of the surface wave data (Schutt et al., 2008), and convective modeling of the Yellowstone plume (Lowry et al., 2000). Our results are relatively insensitive to the depth of the bottom of the plume layer due to the small sensitivity of the phase velocity data to structure below 120 km depth, as shown by Fig. A2. 4) The mantle below the plume layer is assigned the velocity profile predicted by a 1320 °C potential temperature adiabatic mantle with a grain size of 5 mm.

Section 2. Converting Temperature and Melting to S-wave Velocity

Because melt porosity reduces rock velocities (Kreutzmann et al., 2004; Schmeling, 1985; Schutt and Humphreys, 2004; Takei, 2000), the melt porosity of super-solidus regions is quantified as a function of depth. Equilibrium melt porosities are calculated using one-dimensional Darcy law porous flow equations with a melting source-term (Turcotte and Schubert, 2002), as detailed in Section 3. The most important parameters in this calculation are the permeability and the parametric form of the solidus. The permeability is calculated using a power law relation where the grain size is the independent variable (Turcotte and Schubert, 2002). The solidus and hence melt production rate is specified using the dry mantle solidus (Hirschmann, 2000). The dry solidus is appropriate because any volatiles in the plume would be rapidly removed during the extensive melt extraction observed along the YHT (Schutt and Humphreys, 2004). The

melt porosities are displayed as contours in the two-dimensional probability image that shows the trade-off between the grain-size and excess temperature of the plume layer (Fig. 2d,e). The greatest melt-porosity is <1%: consistent with global geochemical constraints that suggest upper mantle melt porosity rarely exceeds 1% (McKenzie, 1984). Above the 52 km depth of the lithosphere-plume layer boundary, we assume that the melt is no longer percolating along grain boundaries, but is channelized (Aharonov et al., 1997) and hence does not volumetrically perturb the velocity field.

Next, the melt porosities and temperature in the plume layer are translated into shear-wave velocities. Translation of the melt porosities into shear-wave velocity reductions is equivocal. For a 1% melt porosity, three studies suggest a corresponding 2% shear-wave velocity reduction (Kreutzmann et al., 2004; Schmeling, 1985; Takei, 2000), while one study suggests a 7.9% velocity reduction (Hammond and Humphreys, 2000a). Because our equilibrium melt porosities are <1%, we find that our excess temperature estimates are not very dependent upon which melt-velocity scaling relation is used. To translate our one dimensional thermal model into velocities, two different anelastic velocity models are tested. The first (NGSS) method is based upon a non-grain size sensitive theoretical anelastic model (Karato, 1993), and has been fairly commonly used in the seismic literature (Goes et al., 2004; Goes et al., 2000; Goes and van der Lee, 2002; Ritzwoller et al., 2004). The second (GSS) method is based upon a grain size sensitive phenomenological fit to laboratory data (Jackson et al., 2002), and is described in section 4. Both the theoretical and laboratory based anelasticity models require the specification of the poorly constrained volume of activation (V^*) (Karato and Jung, 2003) that scales how the seismic attenuation (hence anelasticity) decreases with respect to depth. Estimates of V^* range from 3-25 cm³/mol (Li et al., 2003). For our best estimate of excess temperature, we assume a V^* of 14 cm³/mol (Faul and Jackson, 2005b; Karato and Jung, 2003). This value is chosen both because it is the center of the range of reported values, and also for comparison with other studies that map velocity to temperature (Cammarano et al., 2003; Goes et al., 2000). Fig A3 presents excess temperature estimates for the various values of V^* . Obviously, V^* is a very important parameter and a firmer consensus on its correct value will be very useful.

The mean grain size in the plume affects both the melt porosity, and for the GSS model, the anelasticity. While it would be ideal to have xenoliths from a plume and/or asthenospheric layer from which grain size could be inferred, to our knowledge, no xenoliths from a plume layer or asthenosphere exist. Some estimates of grain size are discussed in Section 5.

Section 3. Melt Porosity Calculation

The mean equilibrium melt porosity in our thermal plume model is calculated using the one-dimensional porous flow equations (Turcotte and Schubert, 2002). The relative velocity between the melt and matrix is

$$(1) \quad v_l - v_s = \frac{b^2 \phi (\rho_s - \rho_l)}{24\pi\mu}$$

where v_l and v_s are the upward velocities of the liquid and solid, b is the grain size, μ is the melt viscosity, ϕ is the melt porosity by volume, and ρ_s and ρ_l are the solid and melt densities. We use the following parameter values: $\rho_s = 3.27 \text{ km/m}^3$, $\rho_l = 2900 \text{ kg/m}^3$, and $\mu = 3 \text{ Pas}$. Note that eqn. 1 is dependent upon grain size because a power law relation between melt porosity and permeability is being used.

After some algebra, the solution for the melt porosity with respect to depth is given as equation 9-220 in (Turcotte and Schubert, 2002). Grain size is an independent variable in our calculations, but the other

parameters are fixed to the following quantities: heat capacity of melt is 1.3×10^3 J/kg-K, the Clapeyron slope for the solidus is 9.1×10^6 Pa/K, and the latent heat of melting is 320×10^3 J/kg.

Section 4. Anelastic shear velocity models

The theoretical non grain-size sensitive anelastic model derivation is well known and we refer the reader to the original sources (Karato, 1993; Minster and Anderson, 1981). The relevant parameter values for the Q model are taken from previous studies (Goes et al., 2000; Sobolev et al., 1996) which derived the following parameter values by calibrating the anelastic velocity model to seismic Q constraints. The values are: $A=0.149$ (pre-exponential constant), $a=0.15$ (seismic frequency dependence), $V^*=14 \text{ mole/cm}^3$ (activation volume), $E^*=510$ kJ/mole (activation energy). An anharmonic velocity field is needed for this model too; this is calculated from (Schutt and Leshner, 2006).

The phenomenological grain-size sensitive anelastic model is an extended Burgers model (Faul and Jackson, 2005b). We refer the reader to the reference for the details and only give a brief outline here of the model. Defining the complex compliance

$$(2) \quad J^*(\omega) = \frac{\varepsilon(t)}{\sigma(t)} \|J(\omega)\| e^{-i\phi(\omega)} = J_1(\omega) - iJ_2(\omega)$$

where $\varepsilon(t)$ and $\sigma(t)$ are the time dependent strain and stress amplitudes, $\phi(\omega)$ is the phase lag between the shear strain and stress, and $J_1(\omega)$ and $J_2(\omega)$ are the real and imaginary components of the compliance.

The frequency dependent shear modulus G and strain energy dissipation Q^{-1} are calculated as follows:

$$(3) \quad G(\omega) = \left(J_1^2(\omega) - J_2^2(\omega) \right)^{-1/2}$$

and

$$(4) \quad Q^{-1} = \frac{J_1(\omega)}{J_2(\omega)}$$

with

$$(5) \quad J_1(\omega, d, T, P) = J_u(P) \left(1 + \delta \ln J_u + \frac{\alpha_Q \Delta}{\tau_H^{\alpha_Q} - \tau_L^{\alpha_Q}} \int_{\tau_H}^{\tau_L} \frac{\tau^{\alpha_Q-1}}{1 + \omega^2 \tau^2} d\tau \right)$$

and

$$(6) \quad J_2(\omega, d, T, P) = J_u(P) \left(\frac{\omega \alpha_Q \Delta}{\tau_H^{\alpha_Q} - \tau_L^{\alpha_Q}} \int_{\tau_H}^{\tau_L} \frac{\tau^{\alpha_Q}}{1 + \omega^2 \tau^2} d\tau + \frac{1}{\omega \tau_m} \right)$$

where d is grain size, T is temperature, P is pressure, $J_u(P)$ is the unrelaxed compliance,

$\Delta = (G_U - G_R) / G_R$ with G_R and G_U being the relaxed and unrelaxed shear modulus, τ is the

distribution of relaxation times with τ_L , τ_H and τ_m being the lower and upper and Maxwell times and α_Q is the seismic frequency dependent exponent.

The temperature and grain size dependence of the Maxwell relaxation time is derived from the temperature and grain size dependence of the viscosity $\eta \approx d^m \exp(E/RT)$ and expressed in the preliminary functional form

$$(7) \quad \tau_m = Ad^m e^{E/RT}$$

where A is a constant, E the activation energy, R the gas constant, T absolute temperature, and d grain size with exponent m . To account for both anelastic and viscous behavior, a modified version of Eqn. 1.6 is used

$$(8) \quad \tau_i = \tau_{iR} \left(\frac{d}{d_R} \right)^m e^{\left[\left(\frac{E}{R} \right) \left(\frac{1}{T} - \frac{1}{T_R} \right) \right]}$$

where τ_i are the upper, lower cutoff times and Maxwell times. The parameter τ_{iR} are the values of τ_i at the reference temperature T_R and the reference grain size d_R . The exponent m is allowed to change between the lower and upper cutoff times versus the Maxwell time to reflect the different diffusion distances involved in anelastic versus viscous relaxation.

The effect of pressure upon the modulus is accounted for by scaling the relaxation times by the factor $\exp(PV^*/RT)$ where V^* is the activation volume. Extremal bounds on V^* range from 3 (Li et al., 2003) to 25 (Karato and Jung, 1998) mol/cm^3 with 14 mol/cm^3 being our preferred value (Faul and Jackson, 2005b; Karato and Jung, 2003). This large range reflects uncertainties in the operative deformation mechanism (diffusion versus dislocation), olivine dampness, and experimental uncertainties.

Section 5. Plume layer grain size constraints

For the grain-size sensitive anelastic velocity model, specification of the mean grain size in our plume layer is of first order importance (Faul and Jackson, 2005a). Grain size sensitive anelasticity is independent of the rock mineralogy and thus the mean grain size of the upper mantle mineralogic assemblage (olivine, pyroxene, and garnet/spinel) is the relevant quantity. However, because olivine is the most abundant and well-characterized upper mantle mineral, we shall assess what the mean olivine grain size constraints might be for a layer of plume mantle emplaced beneath a moving lithosphere.

All other things equal, the inverse relation between deviatoric stress and grain size suggests that low stress region such as the asthenosphere would have a larger grain size with respect to higher stress regions like the lithosphere (Evans et al., 2001; Hall and Parmentier, 2003; Jackson et al., 2002; Karato and Wu, 1993; Zimmerman and Kohlstedt, 2004). However, the theoretical constraints are too weak to directly constrain the grain size in the asthenosphere or a plume layer. Furthermore, much of the plume layer is likely above the solidus which may affect the operative deformation mechanism (Holtzman et al., 2003; Zimmerman and Kohlstedt, 2004) and the Ostwald ripening process (Solomatov, 2001).

Unfortunately, the inability of the asthenosphere to propagate magma filled cracks upwards means that xenolith samples from the asthenosphere are probably not available (although kimberlites may nucleate below the asthenosphere (Collerson et al., 2000; Usui et al., 2003)). Thus, the only direct evidence for upper mantle grain size distribution derives from lithospheric xenoliths. In general, the olivine grain sizes

from spinel peridotite lithospheric xenoliths is <0.5-2 mm (Armenti and Tarquini, 2002; Wilshire et al., 1988). This small grain size is thought to manifest the relatively high stresses present in the cooler portion of the lithosphere. However, the deepest lithospheric coarse-grained xenoliths often have mean grain sizes of a few mm (Ben et al., 2001). Based on this, we conservatively estimate the minimum asthenospheric grain size to be 2 mm. If grain sizes are really much smaller, it is conceivable that the Yellowstone plume phase velocities could be explained by an isothermal mantle with extremely small grain sizes in the plume, e.g. 0.1 mm. Given current knowledge that suggests grain size in the upper mantle is roughly correlated with temperature (Hall and Parmentier, 2003), Yellowstone being a pure grain size induced velocity anomaly seems highly unlikely. Indeed, it is more likely that plume grain size is larger than the mantle below it since stresses should be higher in the colder and more viscous ambient mantle.

A final potential constraint is the shear wave quality ($Q_s \equiv 1/\text{attenuation}$) predicted by the anelasticity models. Figs. 2 and A4 shows the attenuation with respect to excess temperature and grain-size predicted by the two anelastic models in the plume layer. For the GSS models, the Q_s contours is very similar to the misfit surface (Fig. 2), so these models cannot be used to independently constrain Q_s values. Note that the NGSS Q_s does not depend on grain size and is always greater than the GSS predicted Q_s .

Supplemental Figure Captions

Figure A1. Chi-squared value for fit of plume layer as a function of grain size and excess temperature for the two anelastic and two melt-velocity scaling models used. Contours show F-test confidence levels, and dashed lines give minimum excess temperature estimate at 95% (long dashed lines), and 68% (short dashed lines) confidence levels. Top left: GSS anelasticity model, with melt porosity scaling of (Kreutzmann et al., 2004) (1% melting causes a 2% V_S reduction). Top right: GSS anelasticity model with melt porosity scaling of Hammond and Humphreys (1% melting causes a 7.9% V_S reduction (Hammond and Humphreys, 2000b)). Bottom figures are same as top, except the NGSS anelasticity model is used. A V^* of 14 cm³/mol and E^* of 510 KJ/mole is assumed for all calculations.

Figure A2. Effects of depth of bottom of plume layer on fit to YHT phase velocity data. Grain size in plume layer is assumed to be 2 mm. Contours and colors both indicate F-test derived confidence bounds.

Figure A3. Activation volume (V^*) effects on excess temperature and grain size estimate. Colors indicate F-test derived confidence bounds. Titles on plots denotes V^* values used in cm³/mol.

Figure A4. Mean Q_S predicted as a function of grain size and excess temperature of plume layer for GSS and NGSS anelasticity models and melt-velocity scaling. Contours show F-test derived confidence bounds. V^* is fixed at 14cm³/mol.

References

- Aharonov, E., Spiegelman, M., and Kelemen, P., 1997, Three-dimensional flow and reaction in porous media: implications for the Earth's mantle and sedimentary basins: *Journal of Geophysical Research*, v. 102, p. 14821-14833.
- Armienti, P., and Tarquini, S., 2002, Power law olivine crystal size distributions in lithospheric mantle xenoliths: *Lithos*, v. 65, p. 273-285.
- Ben, I.W., Barruol, G., and Mainprice, D., 2001, The Kaapvaal craton seismic anisotropy; petrophysical analyses of upper mantle kimberlite nodules, *in* Anonymous, ed., *The Kaapvaal Project; formation and evolution of cratons.*, American Geophysical Union. Washington, DC, United States. 2001.
- Blackwell, D.D., Stelle, J.L., and Carter, L.S., 1991, Heat flow patterns of the North American continent: A discussion of the DNAG geothermal map of North America: Neotectonics of North America, *Geol. Soc. Amer. DNAG Decade Map Volume 1*, p. 498.
- Cammarano, F., Goes, S., Vacher, P., and Giardini, D., 2003, Inferring upper-mantle temperatures from seismic velocities: *Physics of the Earth and Planetary Interiors*, v. 138, p. 197-222.
- Collerson, K.D., Hapugoda, S., Kamber, B.S., and Williams, Q., 2000, Rocks from the mantle transition zone; majorite-bearing xenoliths from Malaita, Southwest Pacific: *Science*, v. 288, p. 1215-1223.
- Evans, B., Renner, J., and Hirth, G., 2001, A few remarks on the kinetics of static grain growth in rocks: *International Journal of Earth Sciences*, v. 90, p. 88-103.
- Faul, U.H., and Jackson, I., 2005, The seismological signature of temperature and grain size variations in the upper mantle: *Earth and Planetary Science Letters*, v. 234, p. 119-134.

- Goes, S., Cammarano, F., and Hansen, U., 2004, Synthetic seismic signature of thermal mantle plumes: *Earth and Planetary Science Letters*, v. 218, p. 403-419.
- Goes, S., Govers, R., and Vacher, P., 2000, Shallow mantle temperatures under Europe from P and S wave tomography: *Journal of Geophysical Research*, v. 105, p. Pages 11153-11169.
- Goes, S., and van der Lee, S., 2002, Thermal structure of the North American uppermost mantle inferred from seismic tomography.
- Hall, C.E., and Parmentier, E.M., 2003, Influence of grain size evolution on convective instability: *Geochemistry Geophysics Geosystems*, v. 4.
- Hammond, W.C., and Humphreys, E.D., 2000a, Upper mantle seismic wave attenuation: Effects of realistic partial melt distribution: *J. Geophys. Res.*, v. 105, p. 10,987-10,999.
- , 2000b, Upper mantle seismic wave velocity: Effects of realistic partial melt geometries: *Journal of Geophysical Research B: Solid Earth*, v. 105, p. 10,975-10,986.
- Hirschmann, M.M., 2000, Mantle solidus: Experimental constraints and the effects of peridotite composition: *Geochemistry Geophysics Geosystems*, v. 1, p. 2000GC000070.
- Holtzman, B.K., Groebner, N.J., Zimmerman, M.E., Ginsberg, S.B., and Kohlstedt, D.L., 2003, Stress-driven melt segregation in partially molten rocks: *Geochemistry Geophysics Geosystems*, v. 4.
- Jackson, I., Fitz Gerald, J.D., Faul, U.H., and Tan, B.H., 2002, Grain-size-sensitive seismic wave attenuation in polycrystalline olivine: *Journal of Geophysical Research*, v. 107, p. ECV 5-1 - 5-16.
- Karato, S., 1993, Importance of anelasticity in the interpretation of seismic tomography: *Geophysical Research Letters*, v. 20, p. 1623-1626.
- Karato, S., and Jung, H., 1998, Water, partial melting and the origin of the seismic low velocity and high attenuation zone in the upper mantle: *Earth and Planetary Science Letters*, v. 157, p. Pages 193-207.
- Karato, S., and Wu, P., 1993, Rheology of the upper mantle: a synthesis: *Science*, v. 260, p. 771-778.
- Karato, S.I., and Jung, H., 2003, Effects of pressure on high-temperature dislocation creep in olivine: *Philosophical Magazine*, v. 83, p. 401-414.
- Kreutzmann, H., Schmeling, H., Jung, H., Ruedas, T., Marquart, G., and Bjarnason, I.T., 2004, Temperature and melting of a ridge-centered plume with application to Iceland. Part II: Predictions for electromagnetic and seismic observables: *Geophysical Journal International*, v. 159, p. 1097-1111.
- Li, L., Weidner, D.J., Mei, S., Raterron, P., Chen, J., and Durham, W., 2003, A Search for Olivine Activation Volume: *Geophysical Research Abstracts*, v. 5.
- Lowry, A.R., Ribe, N.M., and Smith, R.B., 2000, Dynamic elevation of the Cordillera, western United States: *Journal of Geophysical Research B: Solid Earth*, v. 105, p. 23,371-23,390.
- Lum, C.C.L., Fitton, J.G., Leeman, W.P., Foland, K.A., and Kargel, J.A., 1989, Isotopic variations in continental basaltic lavas as indicators of mantle heterogeneity: examples from the western US Cordillera: *Journal of Geophysical Research*, v. 94, p. 7871-7884.
- McKenzie, D.M., 1984, The generation and compaction of partially molten rock: *J. Petrol*, v. 25, p. 713-765.
- McQuarrie, N., and Rodgers, D.W., 1998, Subsidence of a volcanic basin by flexure and lower crustal flow: the eastern Snake River Plain, Idaho: *Tectonics*, v. 17, p. 203-220.

- Minster, J.B., and Anderson, D.L., 1981, A mode of dislocation-controlled rheology for the mantle: *Philosophical Transactions, Royal Society of London, A*, v. 299, p. 39.
- Ritzwoller, M.H., Shapiro, N.M., and Zhong, S.J., 2004, Cooling history of the Pacific lithosphere: *Earth and Planetary Science Letters*, v. 226, p. 69-84.
- Saito, M., 1988, DISPER80: A subroutine package for the calculation of seismic normal-mode solutions, *in* Doornbos, D.J., ed., *Seismological Algorithms: Computational Methods and Computer Programs*: San Diego, CA, Academic, p. 293-319.
- Schmeling, H., 1985, Numerical models on the influence of partial melt on elastic, anelastic and electric properties of rocks. Part I: elasticity and anelasticity: *Physics of the Earth & Planetary Interiors*, v. 41, p. 34-57.
- Schutt, D.L., Dueker, K., and Yuan, H., 2008, Crust and upper mantle velocity structure of the Yellowstone hot spot and surroundings: *Journal of Geophysical Research*, v. 113, p. doi:10.1029/2007BJ005109.
- Schutt, D.L., and Humphreys, E.D., 2004, P and S Wave velocity and Vp/Vs in the wake of the Yellowstone hotspot: *J. Geophys. Res.*, v. 108, p. doi:10.1029/2003JB002442.
- Schutt, D.L., and Leshner, C.E., 2006, The effects of melt depletion on the density and seismic velocity of garnet and spinel lherzolite: *Journal of Geophysical Research*, v. 111, p. doi:10.1029/2003JB002950.
- Sobolev, S., V., Zeyen, H., Stoll, G., Werling, F., Altherr, R., and Fuchs, K., 1996, Upper mantle temperatures from teleseismic tomography of French Massif Central including effects of composition, mineral reactions, anharmonicity, anelasticity and partial melt: *Earth and Planetary Science Letters*, v. 139, p. Pages 147-163.
- Solomatov, V.S., 2001, Grain size-dependent viscosity convection and the thermal evolution of the Earth: *Earth and Planetary Science Letters*, v. 191, p. 203-212.
- Takei, Y., 2000, Acoustic properties of partially molten media studied on a simple binary system with a controllable dihedral angle: *Journal of Geophysical Research*, v. 105, p. 16,665-16,682.
- Turcotte, D., and Schubert, G., 2002, *Geodynamics*, Cambridge University Press, 402-405 p.
- Usui, T., Helmstaedt, H., Nakamura, E., Kobayashi, K., and Maruyama, S., 2003, Fate of the subducted Farallon plate inferred from eclogite xenoliths in the Colorado Plateau: *Geology*, v. 31, p. 589-592.
- Waite, G., Smith, R.B., and Allen, R.M., 2006, Vp and Vs structure of the Yellowstone Hotspot upper mantle from teleseismic tomography: Evidence for an upper mantle plume: *Journal of Geophysical Research*, v. 111, p. doi: 10.1029/2005JB003867.
- Wilshire, H.G., Meyer, C.E., Nakata, J.K., Calk, L.C., Shervais, J.W., Nielson, J.E., and Schwarzman, E.C., 1988, Mafic and ultramafic xenoliths from volcanic rocks of the western United States: *US Geological Survey Professional Paper*, v. 1443, p. 179.
- Yuan, H., and Dueker, K., 2005, P-wave Tomogram of the Yellowstone plume: *Geophysical Research Letters*, v. 32, p. doi:10.1029/2004GL022056.
- Yuan, H.Y., Stachnik, J.C., and Dueker, K., in preparation, Variations in crustal velocity and thickness along the Yellowstone hotspot track: *Journal of Geophysical Research*.
- Zimmerman, M.E., and Kohlstedt, D.L., 2004, Rheological properties of partially molten lherzolite: *Journal of Petrology*, v. 45, p. 275-298.

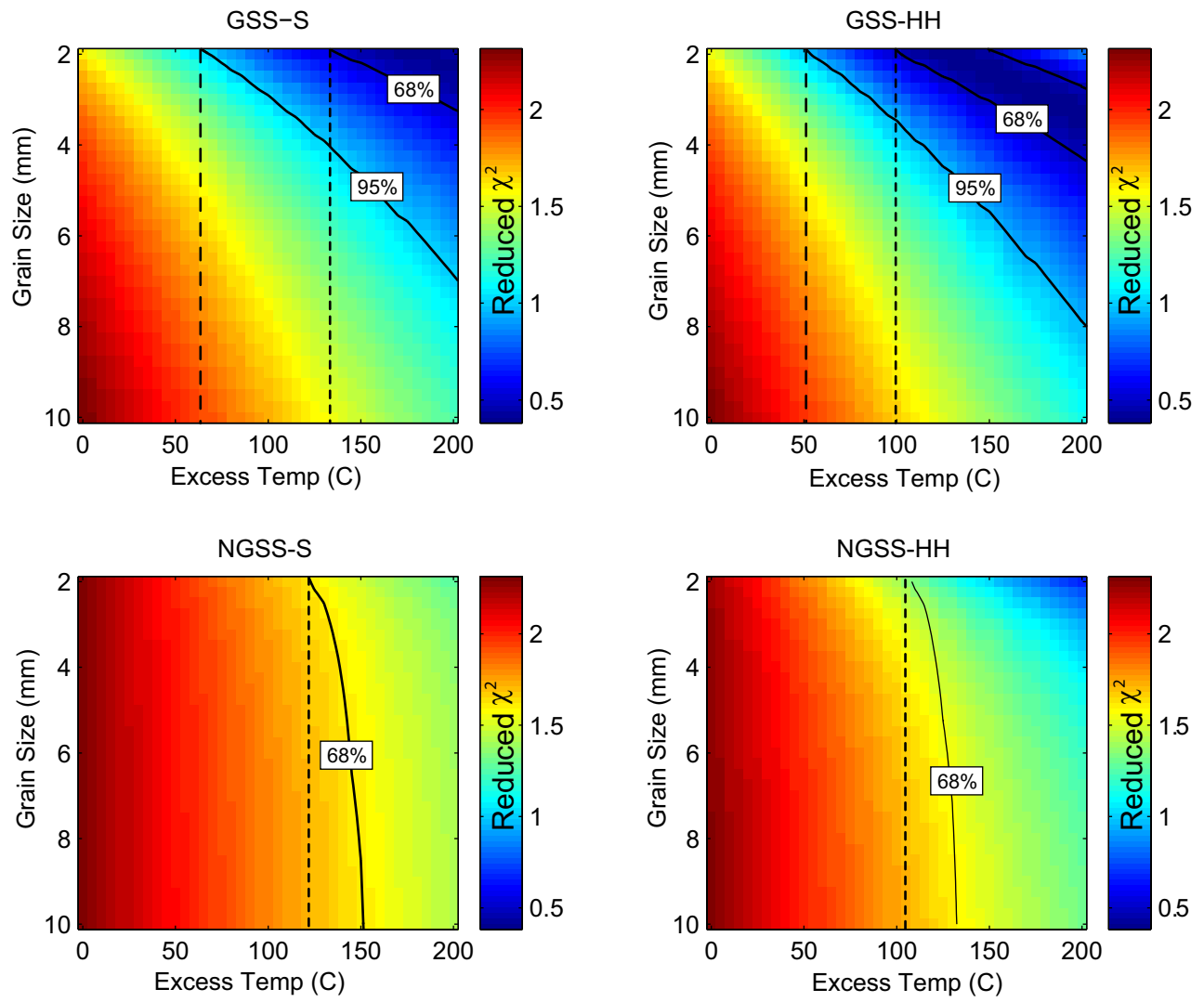


Figure A1.

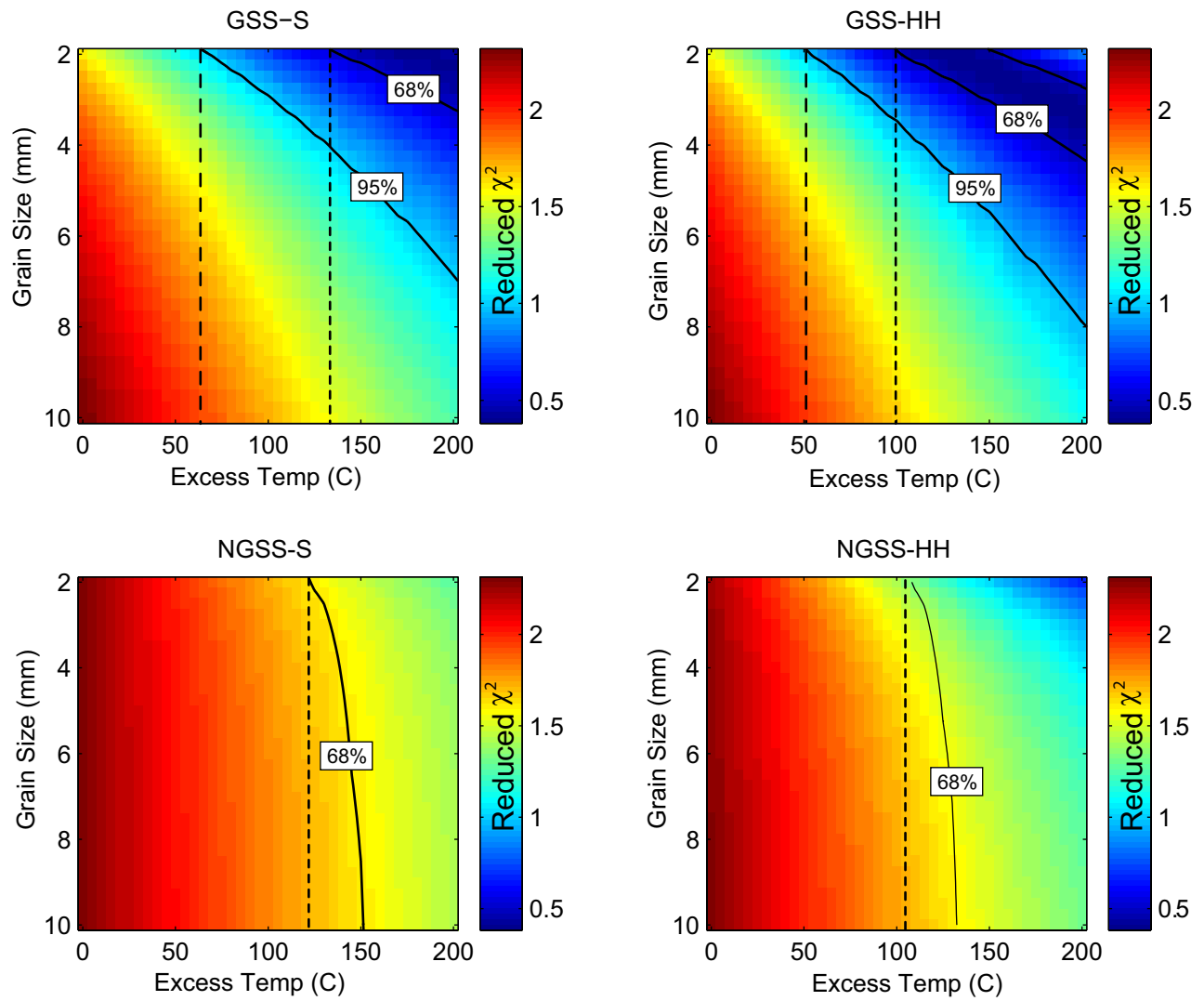


Figure A2.

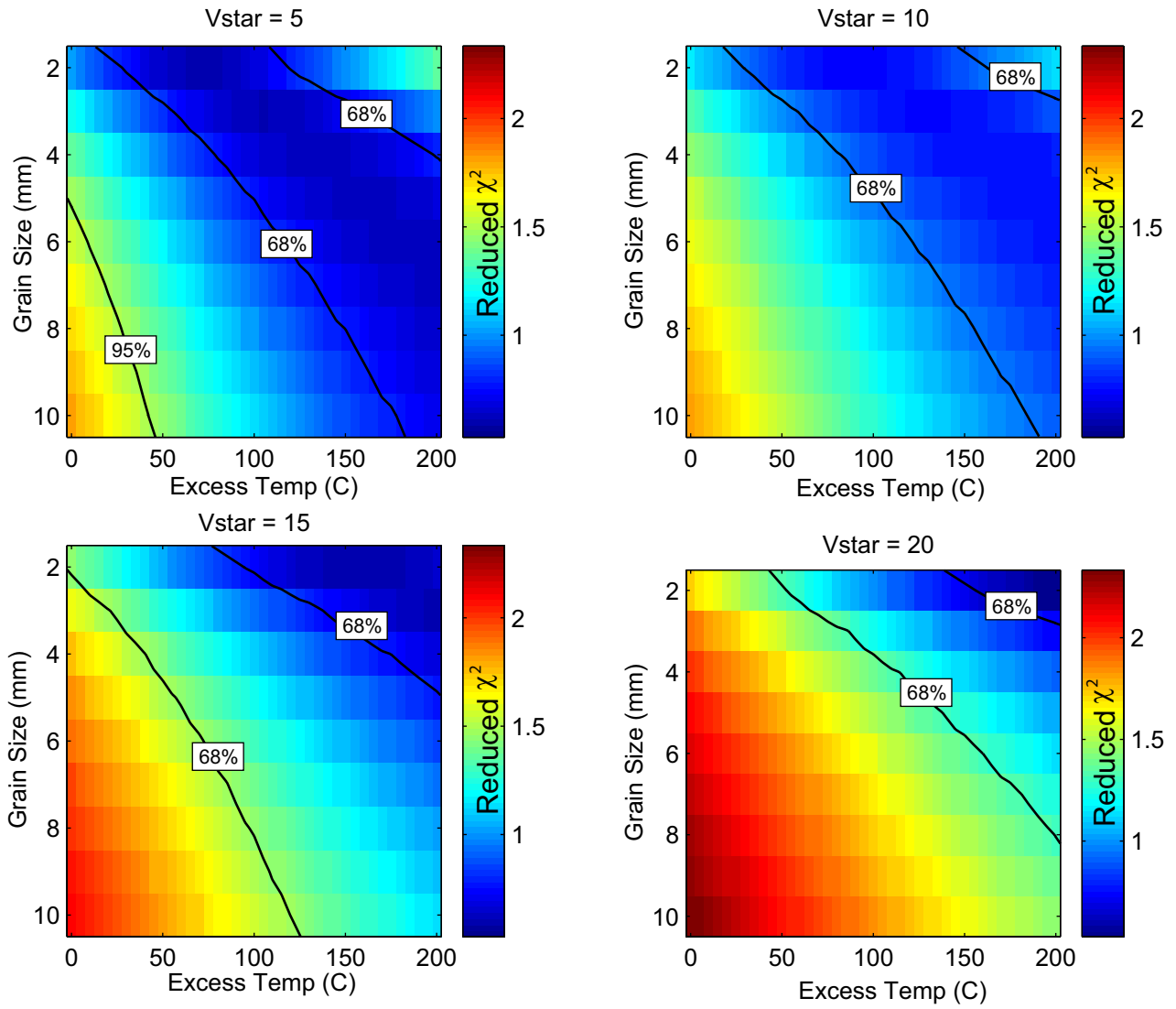


Figure A3.

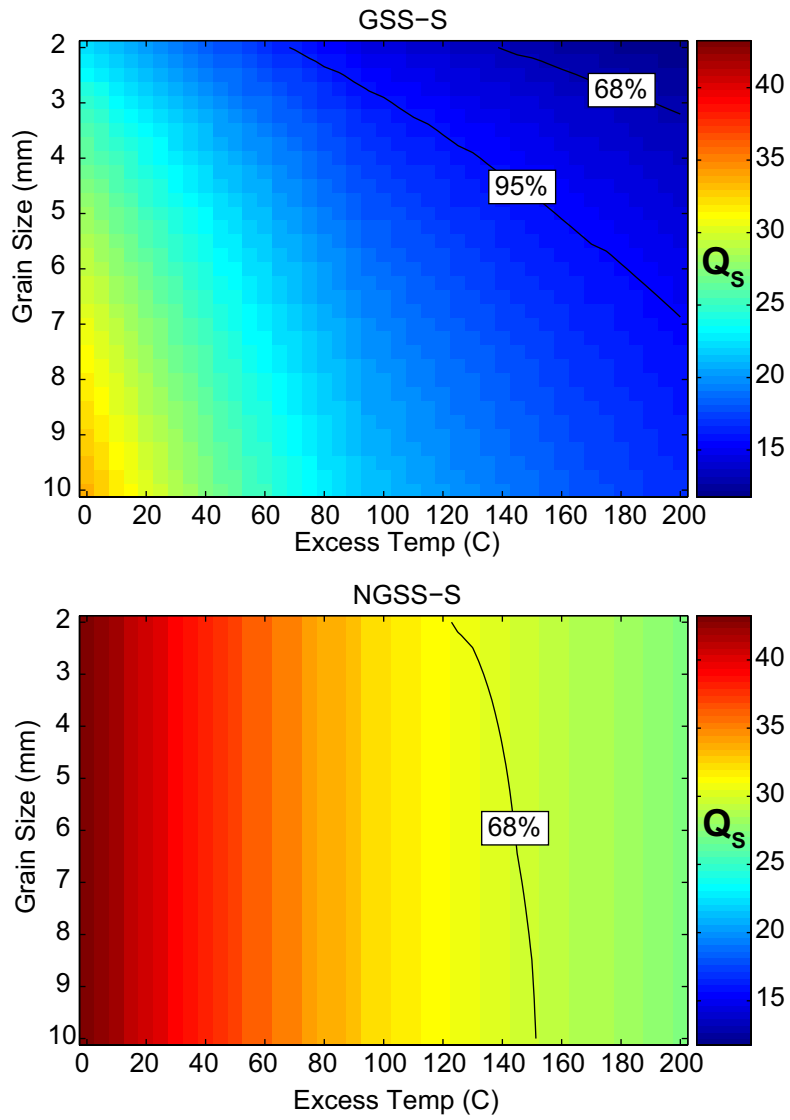


Figure A4.